SSRG International Journal of Mechanical Engineering
ISSN: 2348-8360/ https://doi.org/10.14445/23488360/IJME-V11I6P102

Volume 11 Issue 6, 7-18, June 2024

Original Article

A CFD Analysis of the Flow Structure Inside an R141b Ejector to Identify the Internal Flow Variations in its Design and Off-Design Working Modes

Devendra Kumar Patel[1], M. Anoop Kumar[2]

[1,2]*School of Mechanical Engineering, VIT Vellore, Tamil Nadu, India*

[1]*Corresponding Author : devendrakumar.patel@vit.ac.in*

Received: 02 April 2024 Revised: 14 May 2024 Accepted: 06 June 2024 Published: 30 June 2024

Abstract *- A CFD analysis on an R141b ejector is performed to understand the flow variations at the selected internal sections in its design and off-design modes of operation. The flow inside an ejector with given conditions is numerically simulated, and its correctness is verified with experimental results. Further, the verified numerical model is used to simulate the varying modes of working of the ejector by changing its back pressure (P_b). Seven vertical sections were considered in the flow domain to study the variations in flow parameters. Contours of Mach number and streamlines of the flow were analyzed to understand the varying modes of working of the ejector. A study of the variations in velocity, pressure, temperature, and density along the ejector axis showed that the flow patterns are similar in all modes until the entry of the constant area missing section. After that, in critical mode, the variations are abrupt due to a shock wave, while in other modes, the variations are smooth. Secondary flow velocity at the inlet vertical section decreased from 6.04m/s for P_b=0.05MPa to -3.44 m/s for P_b=0.09MPa. This variation at a vertical section at the primary nozzle outlet is 5.6m/s and 0.07m/s, respectively. In different vertical sections in a constant area mixing chamber, the variations in velocity revealed the momentum exchange happening in the entrainment process.*

Keywords *- Ejector refrigeration, Critical and subcritical modes, Entrainment ratio, CFD, R141b refrigerant, Design and off-design operation, Internal study, Mach number, Streamlines, Velocity variations.*

1. Introduction

An ejector is a flow device used to entrain and compress or pressurize a secondary flow by using an expanding, high-pressure primary flow. They are used in varying industries for pumping, draining, purging, etc. [1]. One of the other major applications of ejector is to produce a refrigeration effect in a thermally driven refrigeration system called Ejector Refrigeration System (ERS) [2-4]. In ERS, the ejector acts as a thermal compressor in place of the mechanical compressor used in the Vapour Compression Refrigerant System (VCRS). The heat energy required for generating high-pressure primary flow required in ejector operation can be extracted from industrial waste heat sources, solar thermal collectors, etc. [5-10]. Thus, ERS promises to be a means of sustainable refrigeration.

However, ERS is not used widely due to many of its inherent drawbacks. Of these, the major drawback is the poor performance of the ejector at off-design operating conditions [1]. This is due to the complicated flow phenomenon occurring in the ejector, as explained in the later section. In order to design the ejector better, a better understanding of ejector flow is needed. This research investigates, by using CFD, the variation in internal flow parameters at defined sections when the ejector is working in its design as well as off-design working modes.

A lot of research has been carried out on ejector flow and ejector working especially for refrigeration applications. Many of this research are either thermodynamic analyses or experimental investigations. The analysis of the ejector working at different operating conditions, the effect of refrigerant used, the performance of the ejector, the ejector refrigeration system etc., are widely reported.

Another group of studies focused on CFD analysis of ejector flow. The effect of operating parameters on ejector performance in terms of entrainment ratio is widely reported. Geometry optimization of the ejector is also investigated. The next two paragraphs give a literature study of the topic, followed by a discussion of the research gap identified and the research objectives defined for this study.

B.J Huang et al. [11] predicted the ejector performance under varying generator pressure using a one-dimensional theoretical model. They also compared the analytical results with the results of experiments conducted using 11 ejectors of varying geometry and refrigerant R141b as the working fluid. It was verified that the 1-D model can quite accurately predict ejector performance. K.O Shestopalov et al. [12] investigated theoretically and experimentally an ejector refrigeration machine operating with R245fa at the design and off-design working conditions. The theoretical results

of ejector performance as well as ejector refrigeration machine were compared with those of experimental results under varying condensing, generating and evaporating temperatures. A good qualitative and quantitative agreement is observed with the results compared. Tongchara Thongtip and Satha Aphornratana [13] presented the design, construction and test of a prototype R141b ejector refrigeration system used as an air conditioner. It is designed to produce a cooling capacity of 4500W with generator temperature in the range of 90-98°C. The condensing temperature was varied from 28°C to 32°C. CFD simulations were employed to design the ejector. The test results showed that the prototype system can work satisfactorily, maintaining 23°C to 25°C inside temperature with a cooling capacity of 4500W. Malek Hamzaoui et al. [14] conducted an experimental study on a low-grade heat-driven ejector cooling system using R245fa. The effect of generator conditions in terms of superheat, pressure and flow rate was investigated on system performance under given condenser and evaporator conditions. It was verified that the ejector works in critical (double-checking) and substantial (single-checking) modes of ejector operation as the generator conditions vary. Selvaraju and Mani [15] investigated the performance of a vapour ejector refrigeration system using R134a as refrigerant and operating under varying temperature conditions. The generator temperature varied between 338K to 363K, the condenser temperature varied between 299K to 305K, and the evaporator temperature varied between 275 K to 285K. Within the above operating range, the entrainment ratio varied between 0.1 to 0.4 to produce a refrigeration effect within 0.5kW. It is reported that the performance of the ejector is highly depending on operating variables. Ian. W. Eames et al. [16] experimented on an ejector refrigeration system working with R245fa as the refrigerant under varying operating conditions. It is reported that the ejector performance drastically reduces as the critical back pressure is exceeded. Results show that COP varied between 0.3 to 0.7 within the range of testing. Charles P et al. [17] investigated experimentally and numerically single-phase parallel ejectors having similar performance curves that could operate individually or simultaneously. The results showed that the tested ejectors in parallel operation retain their performances without any disturbances in their entrainment ratio or critical pressure.

The CFD simulation of an ejector in a CO_2 ejector refrigeration system was performed by [18]to investigate optimizing its geometry. Three geometry parameters viz length of constant pressure mixing chamber, length and diameter of constant area mixing chamber were optimized individually. The relative sensitivity of ejector performance to the 3 ejector geometries was identified. It was observed that the back pressure influences the entrainment ratio of the ejector operating with varying primary pressures. Huaqin Wen and Jia Yan [19] investigated on ejector based multi evaporator refrigeration system. For different modes of ejector operation, CFD simulations were conducted to evaluate the optimum mixing chamber lengths (constant pressure as well as constant area) with fixed and varying area ratios. Results show that the effect of mixing chamber length on ejector performance is minor, while that of area ratio is significant. Haowei Guo et al. [20] performed a CFD simulation for the optimization of ejector nozzle geometry and its Nozzle Exit Position (NXP). With NXP varying from -4 mm to 8 mm, the entrainment ration increased from 0.33 to 0.77 under the tested conditions. The results show that the optimized ejector extends better performance. Egoi Ortego Sampedro [21] investigated a new mixing chamber geometry for an ejector-based refrigeration system using CFD analysis. The results show that with optimization of the mixing chamber, there can be an increase of 120% in cooling capacity compared to conventional geometry. Also, it is reported that the new geometry can lift high the critical condensing temperature by 8°C in the new geometry. Sepehr Sanaye et al. [22] used CFD tools for designing a Combined Ejector-Compressor Refrigeration system (CECR) and optimizing its ejector geometry. It is reported that the COP of CECR is 0.76 while that of conventional Ejector Refrigeration Cycle (ERC)is 0.31. Serjio Croquer et al. [23] compared ejector performance predicted by the thermodynamic model and a corresponding CFD model for different operating conditions. It is reported that the thermodynamic model predicts a high entrainment ratio for double chocking operations and different values of critical pressure in comparison with the CFD model. It is also observed that the CFD model validates that perfect gas assumptions for working fluid can be used for ejector modeling. CFD study of ejectors for identifying suitable experimental conditions that allow reliable ejector cycle operation was carried out by [24]. The flow structure and mixing performance inside the ejector were assessed for varying generator and condenser pressures. The CFD study revealed that the ejector operation is very sensitive to its operating pressures, and CFD can be used for ejector flow analysis and its design.

The literature shows that ejector operation is very sensitive to its operating conditions. An ejector of a given geometry can operate correctly only if the design operating conditions are maintained. This is the main drawback of an ejector preventing its widespread commercial usage, especially in the refrigeration industry where the operating conditions can vary according to climatic conditions. In order to overcome this drawback, the use of multi-ejector systems, ejector nozzle with adjustable spindle etc., is being proposed [1, 21, 25]. The success of these new proposals requires a comprehensive understanding of the refrigerant flow through the ejector. This flow is very complicated in that it can be compressible and turbulent, with many shock wave phenomena occurring. In this context, CFD analysis of ejector flow is a useful method to understand the flow better design of ejectors. Most of the research on ejector flow using CFD existing in open literature focuses on optimizing ejector geometries, observing the variation in contours of Mach number at varying operating conditions, comparing the results of ejector performance by an experimental or thermodynamic model with that of CFD model, etc. Explanation of variations in flow parameters in different working modes of ejectors is not widely reported.

The variations in flow velocity at select vertical sections in the flow domain are hardly reported. This research aims to investigate the variations in contours of Stream lines and Mach number as well as that of the axial flow parameters in design and off-design working modes of the ejector. It also aims to investigate the flow velocity variations happening at select vertical sections in the flow domain. The momentum transfer happening in entrainment phenomena is investigated. In this research, an experimental ejector of given geometry from literature whose performance at specified operating conditions is known is selected for CFD study. This experimental ejector is modeled numerically using CFD tools and simulated using the same experimental input conditions to verify the correctness of the CFD model. Further, this verified CFD model is used to simulate the flow in critical, subcritical and backflow modes of ejector operation. Seven vertical sections were created in the entire geometry of the ejector. In different modes of ejector operation, the variation in flow parameters in the different vertical sections as well as along the ejector axis is studied.

2. Ejector Geometry and Working

The geometry of an ejector is shown in Figure 1(a). It has a primary nozzle, a secondary inlet, a mixing section, and a diffusion section. The mixing section can have a converging section followed by a constant cross-sectional area section. The schematic diagram of the ejector refrigeration system is shown in Figure 1(b). Heat is supplied to the generator to produce high-pressure refrigerant vapor at state 0 at generator pressure (P_g), which is then provided to the primary nozzle of the ejector. The supersonic expansion of the primary flow creates a low pressure at the primary nozzle exit, which facilitates the entrainment of a secondary flow at low pressure (P_e) from the evaporator at state 7. The two flows mix in the mixing section, exchanging energy and momentum. The mixed flow becomes subsonic due to the occurrence of shock waves towards the end of the constant area mixing section. The subsonic flow is further pressurized in the diffuser section and supplied to the condenser at the corresponding pressure (P_c), which is higher than P_e and lower than P_g. Thus, the ejector in ERS acts as a thermal compressor analogous to a mechanical compressor in a Vapour Compression Refrigeration system (VCR).

Ejector performance is expressed in terms of entrainment ratio μ. It is defined as the mass flow rate of secondary flow (m_s) to that of primary flow (m_p).

$$\mu = \frac{m_s}{m_p} \quad (1)$$

The entrainment ratio is depending on the mode of working of the ejector. For a given geometry ejector, it works depending on operating pressures viz Pg, P_e and P_c (or corresponding temperatures). For a given P_g and P_e, it is the outlet pressure P_c which determines the mode of working of the ejector. The outlet pressure is also called back pressure P_b. A typical ejector operating curve is shown in Figure 2 [26]. If P_b is sufficiently less than Pg, the ejector operates as designed and is called critical mode. Here, the ejector is working in the double chocking mode. In a choked flow, the mass flow rate remains constant in a flow through a constrained area, irrespective of a decrease in downstream pressure. The first chocking occurs in primary flow through the nozzle. The second choking occurs from the acceleration of the secondary flow from a stagnant state at the suction part to a supersonic flow along the duct in the mixing chamber. The appearance of the second choking depends directly on P_b. Up to a certain value of back pressure called critical back pressure (P_b*), both the primary and the secondary flows are chocked, causing constant mass flow rates of primary and secondary flows. As a result, μ remains constant. However, if P_b increased to P_b*, primary flow is chocked but not secondary flow. Thus, the mass flow rate of secondary flow decreases sharply as P_b increases further. This is called the subcritical mode of operation or single chocking mode of operation. The entrainment ratio becomes zero when the back pressure becomes P_{b0} and a further increase in P_b leads to backflow of the secondary stream and malfunction mode of operation.

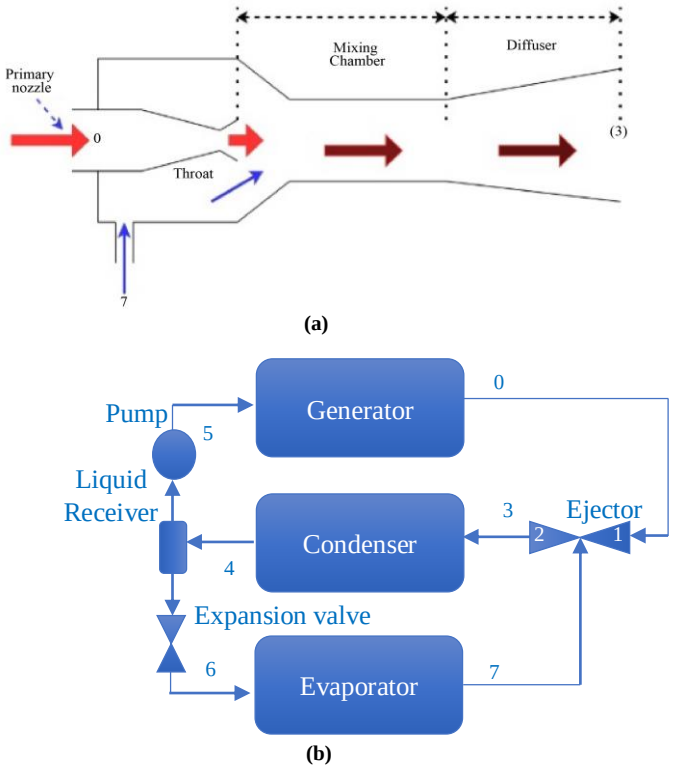

Fig. 1(a) Ejector geometry, and (b) Ejector refrigeration system.

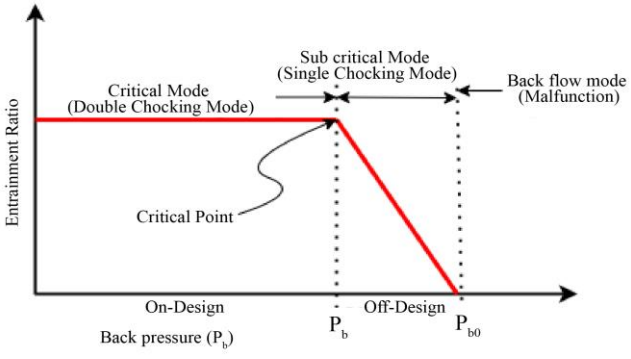

Fig. 2 Ejector operating curve

3. Ejector Geometry and CFD Model

In order to study the variation in internal flow parameters at different modes of operation of an ejector, the ejector experimented by Huang et al. [11] is selected for numerical analysis as it is a well-explained and referred literature. Most of the CFD studies on ejectors report that two-dimensional axisymmetric analysis can give accurate results [13][24][27]. Hence, 2D axisymmetric geometry is considered in this study. The dimensions of the AB ejector by Huang et al., as shown in Figure 3, are considered. The domain consists of a primary inlet, a secondary inlet, an ejector outlet, an ejector outer wall, a primary nozzle wall, and the axis, as explained in Figure 1(a). The primary nozzle inlet was defined as the primary inlet. The secondary flow is entrained through an annulus concentrically with the primary flow. Hence the secondary inlet section is above that of the primary inlet in the 2D geometry. The outlet flow section is defined as an ejector outlet. The ejector main body, as well as primary nozzle bodies, are defined as adiabatic walls. The centerline section about which axisymmetric geometry is defined is considered as the axis.

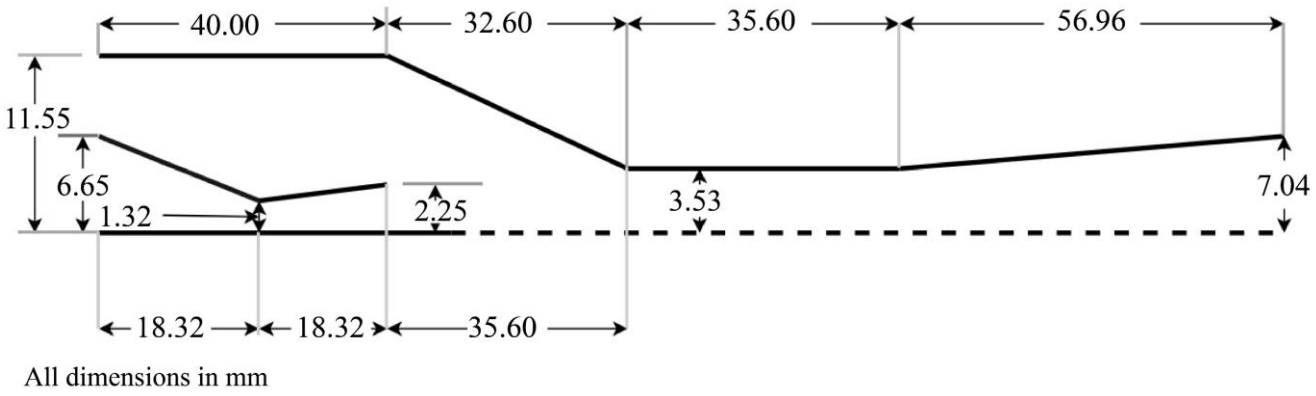

Fig. 3 Axisymmetric ejector dimension

The commercial software ANSYS FLUENT 2020 R2 is used for the modeling. Geometry was created using space claim. A structured mesh of over 30,000 grids was made and shown in Figure 4. The flow is considered steady, compressible, and turbulent. A realizable k-Ɛ model with a pressure-based solver was used. Adiabatic walls with no slip conditions were applied. Pressure inlet and outlet boundary conditions were applied. The solution was considered convergent when the relative residuals were within 10^{-6} for all unknown variables. Refrigerant R 141b is the working fluid.

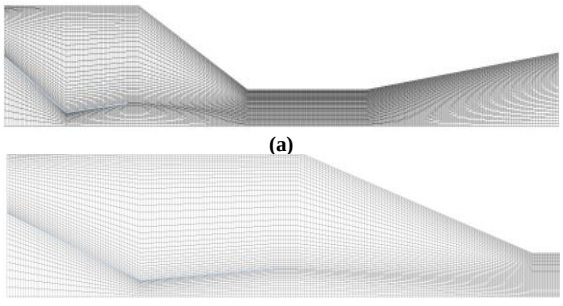

(a)

(b)

Fig. 4 2D axisymmetric grid structure (a) Flow domain, and (b) Enlarged view.

The flow through the ejector is compressible, viscous and turbulent. It should essentially satisfy the equations of continuity, momentum and energy, which are given in their general form below [24].

Continuity:

$$\frac{D_\rho}{D_t} + \rho div\, u = 0 \tag{2}$$

Momentum:

$$\rho \frac{D_u}{D_t} = \rho g - \nabla p + \nabla \tau_{ij} \tag{3}$$

Energy:

$$\rho \frac{D_h}{D_t} = \frac{D_\rho}{D_t} + div(k \nabla T) + \tau_{ij} \frac{\partial u_i}{\partial x_j} \tag{4}$$

Where the stress tensor τ_{ij} is given by:

$$\tau_{ij} = \mu \left(\frac{\partial v_i}{\partial x_j} + \frac{\partial v_j}{\partial x_j} - \frac{2}{3} I\, div\, u \right) \tag{5}$$

First of all, to validate the numerical model developed, the same boundary conditions as Huang et al. experimented for this ejector geometry were applied in the simulation. Pressure inlet and outlet boundary conditions were applied with P_g=0.4MPa, P_e=0.04MPa, and P_b= 0.06 MPa. Thermo-physical properties of the working fluid were obtained from the REFPROP database. Density is modeled using the ideal gas law. Other properties were set constant, corresponding to the pressure and temperature conditions of secondary flow. Simulation of the above-described numerical settings resulted in an entrainment ratio of 0.378. The entrainment ratio obtained in the experimental study for the same input conditions of the reference ejector is 0.392. As the relative error in entrainment ratio between the CFD study and experimental study is only 3.5%, the numerical model developed above can successfully be used for further analysis of the flow happening at the selected ejector's design and off-design operating conditions. A grid independence study was carried out to validate that the above model does not depend on the number of grids in the

mesh. Grid numbers of low, medium, and high density are set as 22523, 46718, and 76204, respectively. Simulations were carried out to get the respective entrainment ratios, as shown in Table 1. The simulation model developed is independent of grid numbers as the variations in the entrainment ratio are negligibly small. Mesh with low grid intensity is selected for further simulation studies.

Table 1. Grid independent test of numerical model

No. of Grids	Entrainment Ratio
22523	0.3789
46718	0.3814
76204	0.3821

For studying the variations happening in flow parameters in different modes of working of the ejector, seven vertical sections were considered in the flow domain with various horizontal positions (x) starting from the inlet, as shown in Figure 5. Section 1 (x=0) is at the inlet comprising of primary and secondary inlet sections. Section 2 (x=18mm) is at the throat of the primary nozzle extending up in the secondary inlet area. Section 3 (x=36mm) at the end of the primary nozzle. Section 4 (x=72.24mm) and 5 (x=107.8mm) are at the entry and exit of the constant area mixing section. Section 6 is at the beginning of the diffuser section at a 120mm distance. Section 7 (x=164.78mm) is the ejector outlet.

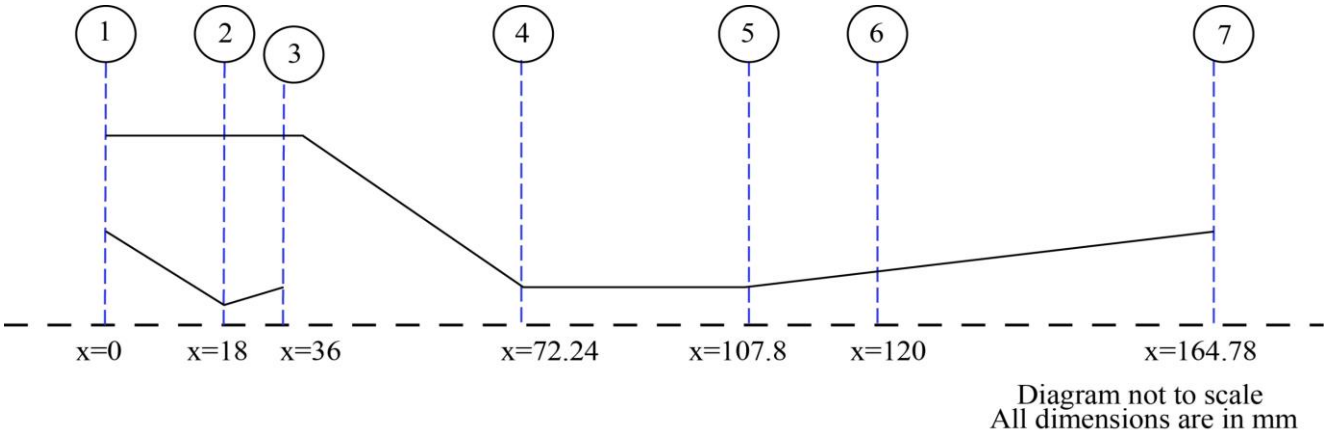

Fig. 5 Internal sections in the flow domain

Variations in flow parameters like velocity, pressure, density, temperature, etc in each section as well as along the axis were obtained in different modes of operation. Also, the contours of Mach number and streamlines were obtained to distinguish the flow at design and off-design modes of working.

4. Results and Discussion

4.1. Ejector Performance

Table 2 shows the various modes of operation of the ejector on varying back pressure. For the back pressure of 0.05MPa and 0.07 MPa, the entrainment ratio remains the same at 0.377. This indicates that the ejector works in critical or design mode. When the back pressure is increased to 0.08MPa, the entrainment ratio reduces to 0.245, and on further increasing the back pressure to 0.85MPa, the entrainment ratio falls to 0.019. Therefore, the ejector works in subcritical mode between 0.07MPa to 0.09 MPa range of the back pressure. Increasing the back pressure to 0.09MPa results in the backflow of refrigerant through the secondary inlet and malfunctioning of the ejector.

4.2. Internal Flow Structure

For the various back pressures mentioned in Table 2, the variations in internal flow parameters were obtained in critical, subcritical and malfunction modes of operations. First, the variations in contours of Mach numbers and streamlines are discussed. Subsequently, the variations in flow parameters at selected sections as well as along the axis were studied.

4.2.1. Variations in Flow Contours

Figure 6 shows the variations in Mach number at various modes of operation. When the back pressure is set to 0.05 MPa, the entrainment ratio is 0.378. The contours of the Mach number for this flow situation are shown in Figure 6(a). A shock train is produced just after the primary nozzle exit and extends to the middle of the constant area mixing section. This is due to the supersonic expansion of the primary flow in the nozzle. The Mach number varies from subsonic (M<1) in the convergent section of the nozzle to sonic(M=1) at its throat and to supersonic(M>1) at the divergent part.

Table 2. Different modes of ejector operation

Back Pressure (P_b or P_c) MPa	Entrainment Ratio (μ)	Mode of Operation	Remarks
0.05	0.378	Critical mode	Double chocking
0.07	0.378	Critical mode	Double chocking
0.08	0.245	Subcritical mode	Single chocking
0.085	0.019	Subcritical mode	Single chocking
0.09	Back flow	Malfunction mode	Malfunctioning

This shows that the primary flow is chocked. The expanding primary flow creates a converging duct in the mixing chamber. The secondary flow is entrained and accelerated to sonic speed in the mixing chamber. Towards the end of the mixing chamber, the two steams mix completely to form a single stream. Due to relatively high pressure in the diffuser outlet, the mixed flow experiences another shock wave, increasing its pressure and decreasing its velocity. This shock is observed at the start of the diffuser section in Figure 6(a). So, the secondary flow is also chocked, and the presence of these two shocks reveals that the ejector is operating in double chocking or critical mode of operation. When the back pressure is increased to 0.07Mpa, the entrainment ratio remains 0.378. The contour of the Mach number as shown in Figure 6(b), is almost the same as that explained previous case. Two shock waves show that the ejector is working in double chocking mode. In the double chocking mode of operation, both the primary and secondary flow are choked, indicating that the respective mass flow rates remain constant irrespective of increasing the back pressure. Thus, in the double chocking or critical mode operation, the entrainment ratio remains the same on varying the back pressure, as shown in Figure 2. When increasing the entrainment ratio to 0.08MPa, the entrainment ratio is reduced to 0.245, indicating that the ejector operation is in subcritical mode. It is evident from the contours of the Mach number shown in Figure 6(c) that there is only one shock train. The second shock at the start of the diffuser section is missing, and it clarifies that the secondary flow is not accelerated to the sonic velocity, and thus, it is not chocked. Thus, the secondary mass flow rate decreases as the back pressure increases. Further increase of the back pressure to 0.085MPa results in an entrainment ratio of 0.019. The contours of Mach shown in Figure 6(d) show that the ejector is working in single chocking mode. Here, the mass flow rate of secondary flow is further reduced, and thus, the entrainment ratio. When the back pressure is set to 0.09 MPa, it is observed that the secondary flow occurs in revere direction. This ensures that the ejector is working in malfunction mode. The corresponding contours of the Mach number are shown in Figure 6(e)

To understand the backflow mode and critical modes of operations, respective streamlines were studied. Figure 7(a) shows the streamlines when the ejector works in malfunction or backflow mode (P_b =0.09MPa). Here, the mass flow rate of the primary inlet is 0.008806 kg/s while that in the secondary inlet is -0.001665kg/s. This indicates that a part of the primary flow is exited back through the secondary inlet. The streamlines at the entry of the mixing chamber show the eddies developed, which rotate anti-clock wise and make a reverse flow through the secondary inlet section. The contours of streamlines in critical mode of operation are shown in Figure 7(b). In the critical mode of operation, the primary mass flow rate is the same as in the above case, and the secondary mass flow rate is 0.003321kg/s. The streamlines through the secondary inlet enter the converging part of the mixing section, make a downward swift, and join the primary flow to enter the constant area mixing section. Thus, the secondary flow can mix with and carry forward by the primary flow.

The contours of Mach number and streamlines explained above flashlight into the entrainment phenomena happening in ejector working. Such explanations are not widely reported in the literature.

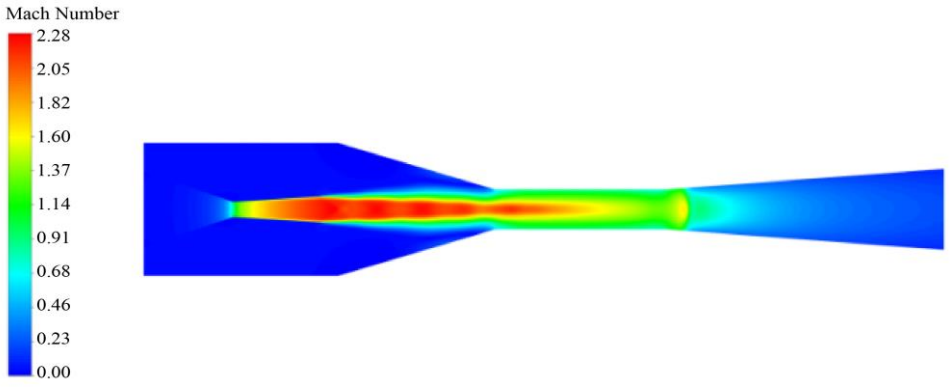

(a)

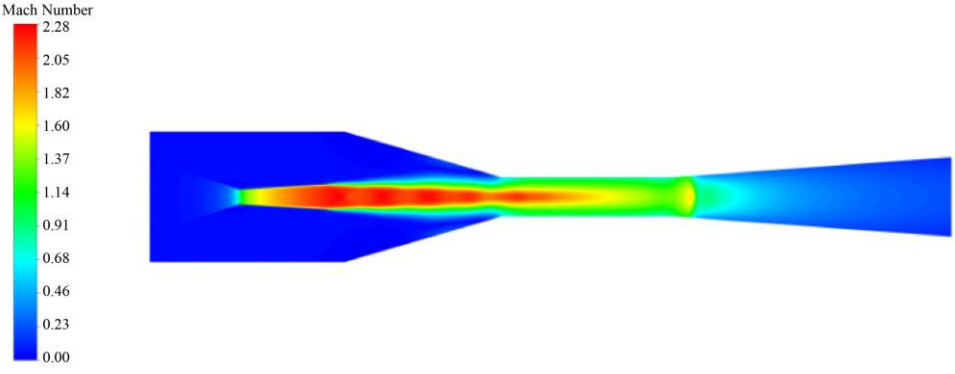

(b)

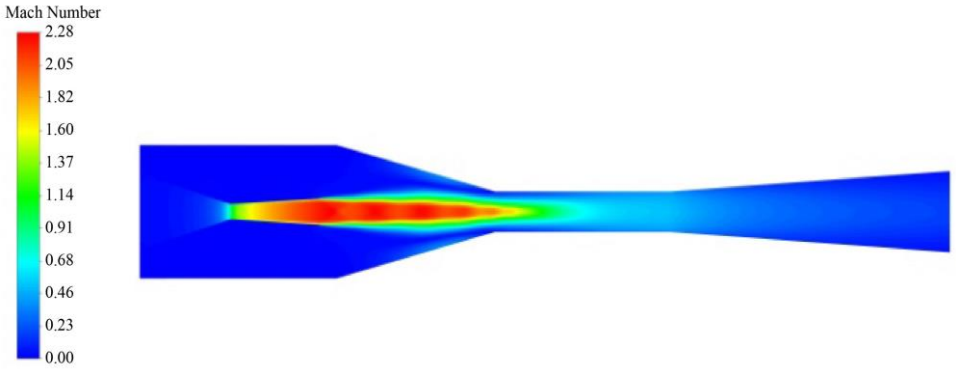

(c)

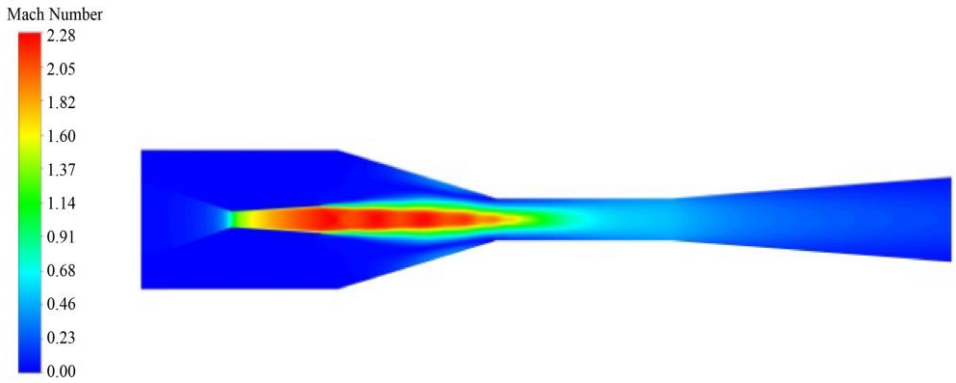

(d)

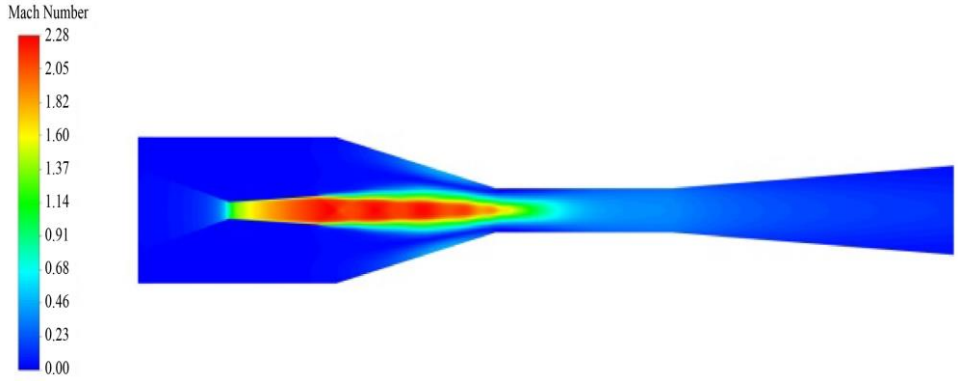

(e)

Fig. 6 Contours of mach number (a) P_b=0.05 MPa, (b) P_b=0.07 MPa, (c) P_b=0.08 MPa, and (d) P_b=0.09 Mpa.

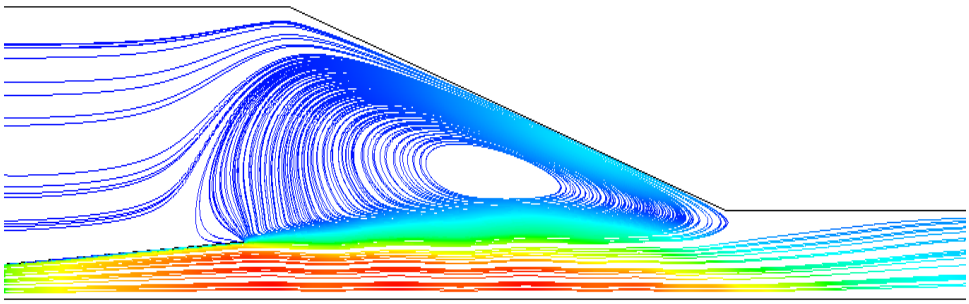

(a)

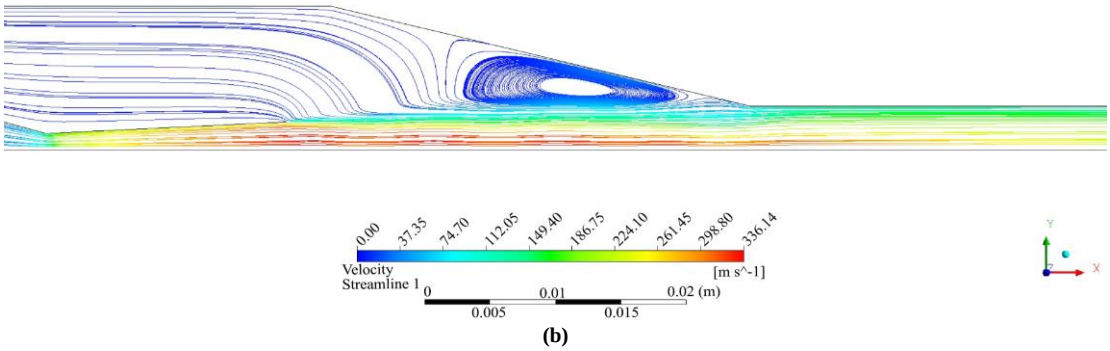

(b)

Fig. 7 Contours of streamline (a) Malfunction mode, and (b) Critical mode.

4.2.2. Variations in Axial Flow Parameters

Figure 8 shows the variation of axial velocity along the axis of the ejector for different outlet pressures and, thus, varying modes of operation. It is observed that a similar velocity profile is exhibited till the entry of the constant area section (x=72.24 mm). The axial velocity is increased from 4m/s to over 330m/s. Within this length, the primary flow is expanded supersonically, producing a series of shock waves. This is clear in the contours of the Mach number shown in Figures 6(a-e). After that, the flow velocity profile varies for different pressures. For the outlet pressure of 0.05MPa, the flow velocity reduces in the constant mixing area section to about 200m/s. After that, a sudden increase to 301 m/s and a steep decrease to 104m/s in axial velocity is observed towards the end of the mixing chamber. It is due to the second normal shock at the entry part of the diffuser section. After this shock wave, the flow velocity is reduced to that of the subsonic region and is further reduced in the diffuser section to about 41.4m/s at the outlet; for the outlet pressures of 0.07 MPa, a similar velocity profile is observed along the axis. However, the occurrence of the second normal shock is shifted left as the outlet pressure increases. Also, the difference in velocity across the normal shock is less (254m/s to 128m/s). There is no second shock wave happening for the sub-critical and back-flow modes of operation. As explained earlier, only one shock train is happening in the primary nozzle. Here, the velocity is drastically reduced in the constant area mixing section (From about 330m/s to about 100m/s) and further in the diffuser section of the ejector (100m/s to 41m/s).

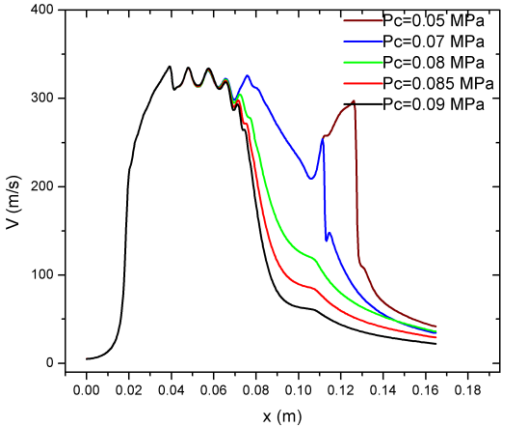

Fig. 8 Variation in axial velocity

Figure 9 shows the variation of static pressure along the ejector axis for different outlet pressures. A trend just opposite to the velocity variation explained above is observed in the case of pressure variation. High-pressure primary fluid is expanded from 0.4MPa to 0.049MPa in the primary nozzle, producing a series of shock waves as risible from the sudden decrease and the subsequent undulations in pressure magnitude. Until the constant area mixing section is entered, the pressure variation profiles are similar for all outlet pressures. After that, the pressure gradually increases in the constant area mixing section and further in the diffuser section to match the applied back pressure. For subcritical and backflow modes, the variation in pressure in the mixing chamber and diffuser is shallow, ranging from 0.07MPa to 0.09 MPa. In critical operations, the pressure is relatively low in the constant area mixing section (0.049MPa). The occurrence of a second normal shock is clear from the sudden increase in pressure at the diffuser entry region. Thereafter, the pressure increases in the diffuser section. A similar trend is observed in the case of axial variation of density, as shown in Figure 10.

Figure 11 shows the variation of static temperature along the axis of the ejector. As the primary flow at 350K is expanded in the nozzle, a sudden drop in temperature to around 280K is observed. After that, the temperature is undulated about this range due to the occurrences of shock trains in the primary nozzle. Thereafter, the temperature increases in the constant area mixing chamber and diffuser section ton. For the critical mode of operation, a steep increase in temperature is visible at the place of the second normal shock.

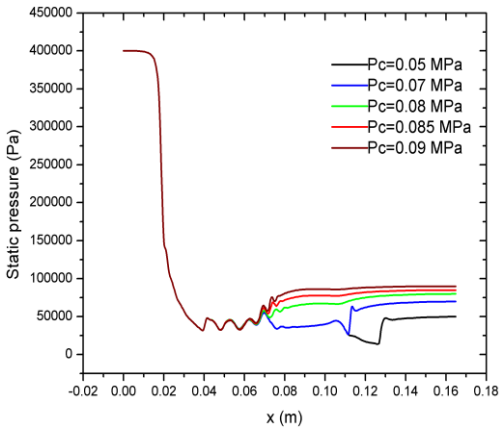

Fig. 9 Variation in static pressure

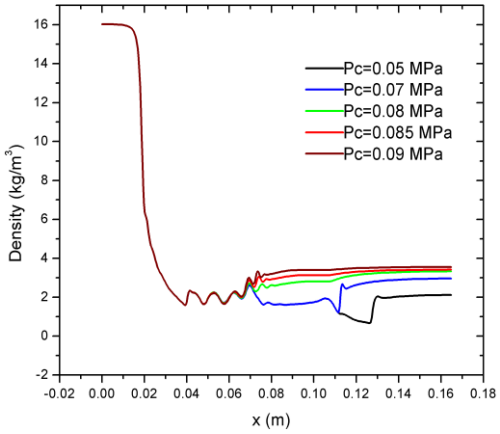

Fig. 10 Variation in density

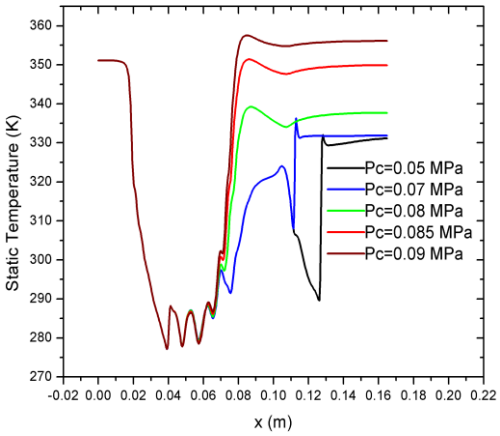

Fig. 11 Variation in static temperature

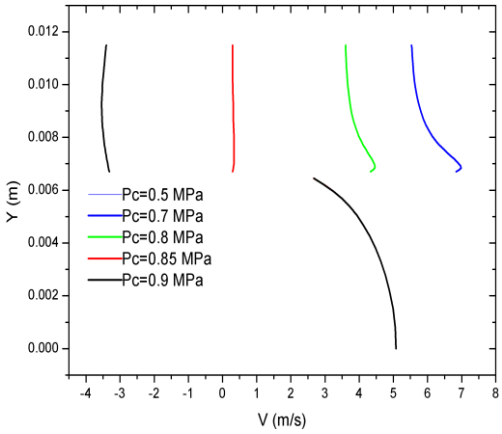

Fig. 12 Axial velocity at section 1

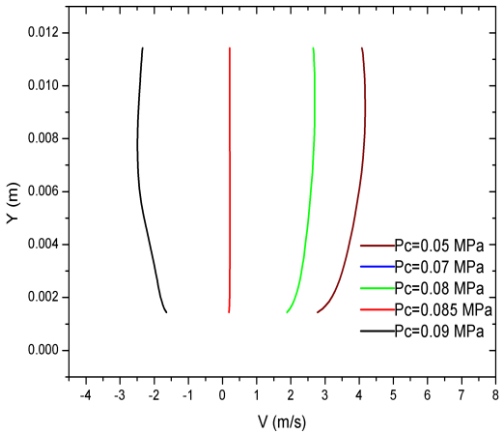

Fig. 13 Axial velocity at section 2

4.2.3. Variations in Flow Velocity at Sections

Velocity variations at different vertical sections in the flow domain, as shown in Figure 5, were analyzed. Figure 12 shows the velocity variation through section 1 at different outlet pressures and, thereby, different modes of ejector operation. The lower semi-parabola represents the flow through the primary nozzle. Remember that it is the half profile of the total flow, as we have considered axisymmetric geometry for the analysis. In section 1, the primary flow is subsonic with a maximum velocity of 5 m/s at the center, and it reduces to 2.5 m/s at the upper section of the primary nozzle.

The primary flow profile remains the same for all the outlet pressures, as it is always choked. However, the secondary flow velocity is different for various outlet pressures. For the outlet pressures of 0.05MPa and 0.07 MPa, the ejector operation is in critical mode, and the secondary velocity is blue. The flow has an average velocity of 6.04 m/s. When the pressure is increased further, the ejector operation becomes subcritical.

That means the secondary flow is not chocked and decreases as the outlet pressure increases. For the outlet pressure of 0.08MPa, the average value of secondary flow velocity is 3.91 m/s, and it reduces to 0.31m/s when the outlet pressure is increased to 0.085MPa. With a further increase in outlet pressure to 0.9 MPa, the average velocity of secondary flow becomes -3.44 m/s, meaning that the ejector is in malfunction or backflow mode of operation.

Velocity variation in section 2 is shown in Figure 13. Here, the profiles of only secondary flows are shown as the average velocity of primary flow (138m/s) in comparison with secondary flow is very large, and it will not enable the distinguishing of secondary flow if plotted together. Here also, the profiles of secondary flow under the critical mode of operation (P_b=0.05MPa, 0.07MPa) are identical and have an average velocity of 3.80 m/s. When the ejector operation becomes subcritical, the average velocity reduces to 2.48 m/s (P_b=0,08MPa) and further to 0.21m/s (Pb=0.085MPa). When the ejector operates in backflow mode (P_b=0.09MPa), the average secondary flow velocity becomes -2.21m/s.

Figure 14 shows the velocity variation in section 3. Here again, the profiles of secondary flow alone are considered as the primary flow is of very high velocity of average 308m/s. For the critical operation conditions, the flow velocity is 3.15m/s on top, increasing to 28m/s towards the lower portion of the secondary inlet section, resulting in an average velocity of 5.60m/s. For the subcritical mode of operation, the average velocity is 4.18 m/s (P_b=0.08MPa) and 0.189m/s (P_b=0.085MPa). For the backflow mode, the average velocity is 0.07m/s. In all the above cases, it is observed that the secondary flow velocity is increased to about 27m/s towards the bottom part of the profile. This increase in velocity towards the bottom part of the secondary inlet can be due to the suction effect created by the highly expanding supersonic primary flow. It will induce a viscous effect on the fluid in the secondary area at the intervening portion and thereby lead to the increase in

velocity of the secondary stream towards the lower part of its passage area. In critical mode, this increased velocity is carried forward, leading to the entrainment of secondary flow, as explained in flow streamlines shown in Figure. In backflow mode this increased velocity is turned back by eddies to move back, leading to malfunctioning of the ejector.

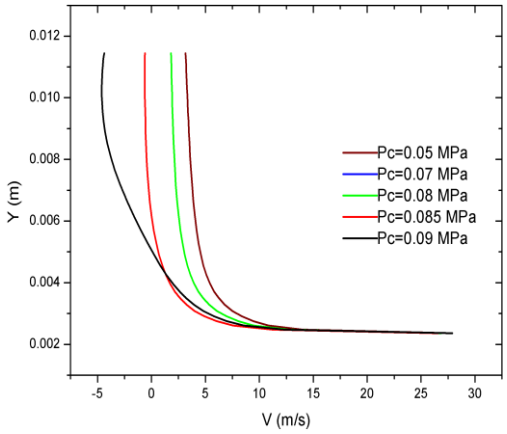

Fig. 14 Axial velocity at section 3

The velocity profile in section 4 is shown in Figure 15. Flow with both primary and secondary streams is considered in this section. For the critical mode of operation, the velocity is at 85 m/s at the upper portion. It increases to 310 m/s towards the middle of the entry of the constant area section, leading to an average velocity of 191m/s. For the subcritical mode of operation, the variations are of a lower magnitude with an average value of 166m/s (P_b=0.08MPa) and 137m/s (P_b=0.085m/s). Since there is significant variation in velocity from the upper part of the profile (secondary flow) to the lower part of the profile (primary flow), it can facilitate the effective momentum transfer between the entrained secondary flow and the supersonic primary flow. For backflow mode, the average velocity is 115.7m/s. Since the secondary flow is not entrained and carried forward, momentum and energy exchange are impossible between primary and secondary flow. In this case, a significant portion of the expanding primary flow is exited through the outlet while a minor part is flown back through the secondary inlet. This type of analysis is exclusive to this investigation.

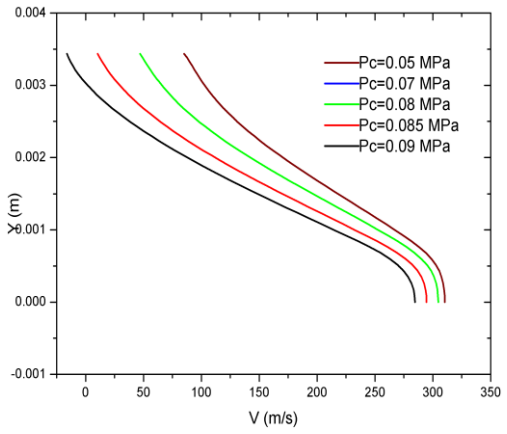

Fig. 15 Axial velocity at section 4

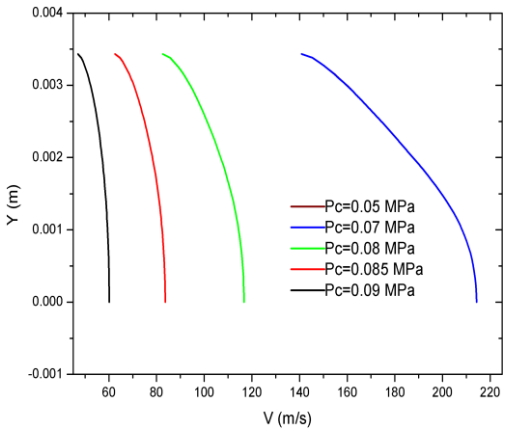

Fig. 16 Axial velocity at section 5

Section 5 is the exit portion of the constant area mixing chamber, and the respective velocity profiles are shown in Figure 16. It is observed that the velocity from the upper part of the profile to its lower does not have a drastic variation, as observed in sections 4 and 5. This indicates that the flow has mixed thoroughly, exchanging energy and momentum. For the critical mode of operation, the average velocity is 182m/s. Since both the primary and secondary flows are chocked in case of critical mode, the velocity profile is the same for both 0.05MPa and 0.07MPa outlet pressures. For other modes of operation, the velocity decreases as the outlet pressure increases. For 0.08MPa and 0.085Mpa pressure, the average velocity is 105m/s and 77.1m/s, respectively. For the pressure of 0.09MPa, the average velocity is 55.18m/s.

Section 6 is in the diffuser part at x=120mm, and the velocity variation in this section is shown in Figure 17. In critical modes of operation, the normal shocks are happening at a position in this section. The velocity across a normal shock is witnessing a sudden increase and decrease, as shown in Figure 8. Hence, the velocity profile at section 6 in critical modes of operation on the position of the velocity peak relative to section 6. For instance, in the case of outlet pressure 0.05MPa outlet, the average velocity is 254.1m/s, which is high because section 6 happens to be at the peak of the normal shock, as seen in Figure 8. On the other hand, for the outlet pressure of 0.07MPa, the average velocity is only 85m/s because section 6 happens to be after the normal shock again, as seen in Figure 8. Hence, in the critical mode of operation, the velocity profiles are not identical for the two outlet pressures, as observed in previous sections. For the outlet pressures of 0.08MPa, 0.085MPa, and 0.09MPa, the average velocity at section 6 is 64.03m/s,49.5m/s, and 37.8m/s, respectively.

Section 7 is at the ejector outlet. In critical modes of operation, the flow becomes subsonic at the start of the diffuser section. In other modes, the flow is already in subsonic mode, as seen in the Mach number plots of Figure 6. As the diffuser increases the pressure and reduces the velocity of a subsonic flow, the velocity profiles are quite low in magnitude, as seen in Figure 18. and it decreases with an increase in outlet pressure. For the outlet pressures of 0.05MPa, 0.07MPa, 0.08MPa,0.085MPa and 0.09MPa, the

respective average velocity at section 7 are 35.2 m/s, 26.5m/s, 22.6m/s,17.7m/sand 13.5m/s.

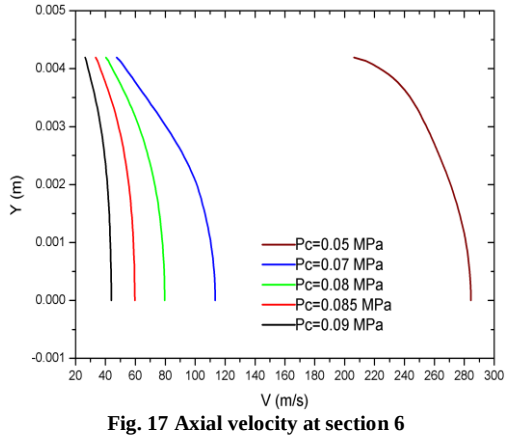

Fig. 17 Axial velocity at section 6

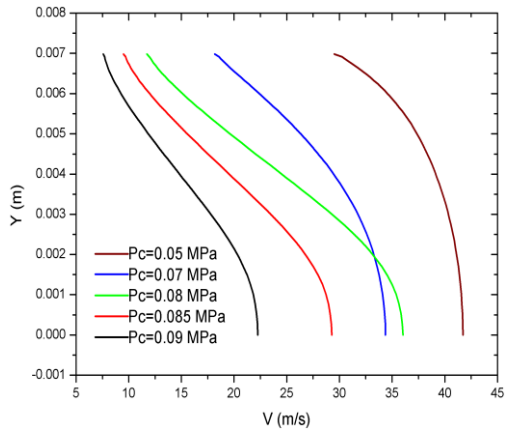

Fig. 18 Axial velocity at section 7

The results discussed above are quite new to the existing literature in this domain. It flashes light into the entrainment phenomena happening in ejector operation. The entrained flow and back flow could be visualized using contours of streamlines.

The momentum exchange analyzed at the constant area mixing section could explain how the two flows exchange energy and momentum to get mixed. This analysis can be used for a better understanding of the ejector flow which in turn can help in its improved design.

5. Conclusion

A numerical study using CFD on a selected R141b ejector is carried out to understand the variations in flow parameters at its design and off-design modes of operation. A numerical model of the ejector flow was created using ANSYS FLUENT tools, and the simulation model was verified using experimental results at P_g=0.4MPa, P_e=0.04MPa, and P_b=0.06MPa. Further simulations were done using this model, varying the Pb and keeping other pressures constant. The ejector was observed to operate in design or critical mode for P_b=0.05 MPa and P_b=0.07 MPa with an entrainment ratio of 0.378. When Pb is increased to 0.08MPa, the entrainment ratio reduces to 0.245 and 0.01 for P_b=0.085, indicating that the ejector operates in subcritical (off-design) mode. Further increase of Pb=0.09Mpa resulted in backflow of the secondary stream and thus malfunctioning of the ejector. The contours of the Mach number in different modes revealed that the ejector operates in double chocking mode for design conditions and single chocking mode for off-design conditions. The contours of streamlines show that the presence of eddies at the converging part of the mixing section regulates the secondary flow entrainment and its back flow at different ejector working modes. The variations in flow properties viz velocity, pressure, temperature, and density along the axis of the ejector showed abrupt variations in critical modes of operation due to the presence of normal shocks in diffuser entry. For other modes, these variations are steep but smooth. A study of the flow velocity at defined vertical sections in the flow domain revealed how the entrainment and backflow take place in respective ejector operation modes. In the secondary inlet section, the average velocity varies from 6.04m/s at the critical mode of operation to -3.44m/s at the backflow mode. In a vertical section at the entry of the constant area mixing section, the difference in velocity between secondary and primary flow can be over 200m/s. This facilitates the exchange of momentum and energy between the two streams in the mixing chamber. At a vertical section at the exit of the constant area mixing chamber, this difference has reduced within 70m/s.

Acknowledgements

The authors acknowledge the support facilitated by VIT University, Vellore, India, in accomplishing this research.

References

[1] Zine Aidoun et al., “Current Advances in Ejector Modeling, Experimentation and Applications for Refrigeration and Heat Pumps. Part 1: Single-Phase Ejectors,” *Inventions*, vol. 4, no. 1, pp. 1-73, 2019. [CrossRef] [Google Scholar] [Publisher Link]

[2] Jianyong Chen et al., “A Review on Versatile Ejector Applications in Refrigeration Systems,” *Renewable and Sustainable Energy Reviews*, vol. 49, pp. 67-90, 2015. [CrossRef] [Google Scholar] [Publisher Link]

[3] Stefan Elbel, and Predrag Hrnjak, “Ejector Refrigeration: An Overview of Historical and Present Developments with an Emphasis on Air-Conditioning Applications,” *International Refrigeration and Air Conditioning Conference*, 2008. [Google Scholar] [Publisher Link]

[4] Mehdi Zeyghami, D. Yogi Goswami, and Elias Stefanakos, “A Review of Solar Thermo-Mechanical Refrigeration and Cooling Methods,” *Renewable and Sustainable Energy Reviews*, vol. 51, pp. 1428-1445, 2015. [CrossRef] [Google Scholar] [Publisher Link]

[5] Dan Nchelatebe Nkwetta, and Jim Sandercock, “A State-of-the-Art Review of Solar Air-Conditioning Systems,” *Renewable and Sustainable Energy Reviews*, vol. 60, pp. 1351-1366, 2016. [CrossRef] [Google Scholar] [Publisher Link]

[6] J.M. Abdulateef et al., “Review on Solar-Driven Ejector Refrigeration Technologies,” *Renewable and Sustainable Energy Reviews*, vol. 13, no. 6-7, pp. 1338-1349, 2009. [CrossRef] [Google Scholar] [Publisher Link]

[7] Farah Kojok et al., "Hybrid Cooling Systems: A Review and an Optimized Selection Scheme," *Renewable and Sustainable Energy Reviews*, vol. 65, pp. 57-80, 2016. [CrossRef] [Google Scholar] [Publisher Link]
[8] Ioan Sarbu, and Calin Sebarchievici, "Review of Solar Refrigeration and Cooling Systems," *Energy and Buildings*, vol. 67, pp. 286-297, 2013. [CrossRef] [Google Scholar] [Publisher Link]
[9] Abdul Ghafoor, and Anjum Munir, "Worldwide Overview of Solar Thermal Cooling Technologies," *Renewable and Sustainable Energy Reviews*, vol. 43, pp. 763-774, 2015. [CrossRef] [Google Scholar] [Publisher Link]
[10] Md Khairul Bashar Shovon et al., "Performance of Ejector Refrigeration Cycle Based on Solar Energy Working with Various Refrigerants," *Journal of Thermal Analysis and Calorimetry*, vol. 141, pp. 301-312, 2020. [CrossRef] [Google Scholar] [Publisher Link]
[11] B.J. Huang et al., "A 1-D Analysis of Ejector Performance," *International Journal of Refrigeration*, vol. 22, no. 5, pp. 354-364, 1999. [CrossRef] [Google Scholar] [Publisher Link]
[12] K.O. Shestopalov et al., "Investigation of an Experimental Ejector Refrigeration Machine Operating with Refrigerant R245fa at Design and Off-Design Working Conditions. Part 2. Theoretical and Experimental Results," *International Journal of Refrigeration*, vol. 55, pp. 212-223, 2015. [CrossRef] [Google Scholar] [Publisher Link]
[13] Tongchana Thongtip, and Satha Aphornratana, "Development and Performance of a Heat Driven R141b Ejector Air Conditioner: Application in Hot Climate Country," *Energy*, vol. 160, pp. 556-572, 2018. [CrossRef] [Google Scholar] [Publisher Link]
[14] Malek Hamzaoui et al., "Experimental Study of a Low Grade Heat Driven Ejector Cooling System Using the Working Fluid R245fa," *International Journal of Refrigeration*, vol. 86, pp. 388-400, 2018. [CrossRef] [Google Scholar] [Publisher Link]
[15] A. Selvaraju, and A. Mani, "Experimental Investigation on R134a Vapour Ejector Refrigeration System," *International Journal of Refrigeration*, vol. 29, no. 7, pp. 1160-1166, 2006. [CrossRef] [Google Scholar] [Publisher Link]
[16] Ian W. Eames, Ali E. Ablwaifa, and Volodymyr Petrenko, "Results of an Experimental Study of an Advanced Jet-Pump Refrigerator Operating with R245fa," *Applied Thermal Engineering*, vol. 27, no. 17-18, pp. 2833-2840, 2007. [CrossRef] [Google Scholar] [Publisher Link]
[17] Charles P. Rand, Michel Poirier, and Sébastien Poncet, "Single-Phase Air Parallel Ejectors: An Experimental and Numerical Study," *International Journal of Refrigeration*, vol. 150, pp. 32-40, 2023. [CrossRef] [Google Scholar] [Publisher Link]
[18] Ruixin Li, Jia Yan, and Christopher Reddick, "Optimization of Three Key Ejector Geometries under Fixed and Varied Operating Conditions: A Numerical Study," *Applied Thermal Engineering*, vol. 211, 2022. [CrossRef] [Google Scholar] [Publisher Link]
[19] Huaqin Wen, and Jia Yan, "Effect of Mixing Chamber Length on Ejector Performance with Fixed/Varied Area Ratio under Three Operating Conditions in Refrigerated Trucks," *Applied Thermal Engineering*, vol. 197, 2021. [CrossRef] [Google Scholar] [Publisher Link]
[20] Haowei Guo, Chen Wang, and Lei Wang, "Optimization of the Primary Nozzle for Design a High Entrainment Ejector in Spacesuit Portable Life Support System," *Applied Thermal Engineering*, vol. 217, 2022. [CrossRef] [Google Scholar] [Publisher Link]
[21] Egoi Ortego Sampedro, "A New Variable Mixing Chamber Ejector: CFD Assessment," *Applied Thermal Engineering*, vol. 208, 2022. [CrossRef] [Google Scholar] [Publisher Link]
[22] Sepehr Sanaye et al., "A Novel Application of Optimization and Computational Fluid Dynamics Methods for Designing Combined Ejector-Compressor Refrigeration Cycle," *International Journal of Refrigeration*, vol. 108, pp. 174-189, 2019. [CrossRef] [Google Scholar] [Publisher Link]
[23] Sergio Croquer, Sébastien Poncet, and Nicolas Galanis, "Comparison of Ejector Predicted Performance by Thermodynamic and CFD Models," *International Journal of Refrigeration*, vol. 68, pp. 28-36, 2016. [CrossRef] [Google Scholar] [Publisher Link]
[24] Yosr Allouche, Chiheb Bouden, and Szabolcs Varga, "A CFD Analysis of the Flow Structure Inside a Steam Ejector to Identify the Suitable Experimental Operating Conditions for a Solar-Driven Refrigeration System," *International Journal of Refrigeration*, vol. 39, pp. 186-195, 2014. [CrossRef] [Google Scholar] [Publisher Link]
[25] Kun Zhang et al., "Experimental Investigation of Adjustable Ejector Performance," *Journal of Energy Engineering*, vol. 138, no. 3, pp. 125-129, 2012. [CrossRef] [Google Scholar] [Publisher Link]
[26] Jianyong Chen, "*Investigation of Vapor Ejectors in Heat Driven Ejector Refrigeration Systems*," Doctoral Dissertation, KTH Royal Institute of Technology, 2014. [Google Scholar] [Publisher Link]
[27] Fahid Riaz, Poh Seng Lee, and Siaw Kiang Chou, "Thermal Modelling and Optimization of Low-Grade Waste Heat Driven Ejector Refrigeration System Incorporating a Direct Ejector Model," *Applied Thermal Engineering*, vol. 167, 2020. [CrossRef] [Google Scholar] [Publisher Link]

Nomenclature

symbols
M- Mach no
P- pressure (MPa)
T-temperature(K)
m-mass flow rate
P_b-back pressure (MPa)
P_{b*}- critical back pressure
P_{bo}- back flow pressure
x-axial position
v-velocity(m/s)
1-7- section no1-7

Abbreviation
ERS-Ejector refrigeration system
VCR-Vapour compression refrigeration
NXP-Nozzle exit position
COP-Coefficient of performance

Subscript
g-generator
e-evaporator
c-condenser
p-primary flow
s-secondary flow

Greek letter
μ-entrainment ratio
τ-stress tensor(Pa)
Ɛ-Turbulent kinetic energy dissipation rate(m^2s^{-3})